EUKARYOTIC CELL, Feb. 2008, p. 368–378 Vol. 7, No. 2
1535-9778/08/$08.00+0 doi:10.1128/EC.00159-07

A *Botrytis cinerea* Emopamil Binding Domain Protein, Required for Full Virulence, Belongs to a Eukaryotic Superfamily Which Has Expanded in Euascomycetes[▽]

A. Gioti,* J. M. Pradier, E. Fournier, P. Le Pêcheur, C. Giraud, D. Debieu, J. Bach, P. Leroux, and C. Levis

UMR1290 BIOGER-CPP, INRA, Route de St-Cyr, 78026 Versailles, France

Received 3 May 2007/Accepted 27 November 2007

A previous transcriptomic analysis of 3,032 fungal genes identified the *Botrytis cinerea PIE3* (Bc*PIE3*) gene to be up-regulated early in planta (A. Gioti, A. Simon, P. Le Pêcheur, C. Giraud, J. M. Pradier, M. Viaud, and C. Levis, J. Mol. Biol. 358:372–386, 2006). In the present study, Bc*PIE3* was disrupted in order to determine its implication in pathogenicity. BcPIE3 was shown to be a virulence factor, since the ΔBcPIE3 mutant was blocked during the colonization of tomato and bean leaves, giving lesions reduced in size by at least 74%. Within the emopamil binding domain (EBD), BcPIE3 shows significant structural similarities to mammalian emopamil binding proteins (EBPs). Mammalian EBPs function as sterol isomerases, but an analysis of the sterol content and the results of growth inhibition experiments with the ΔBcPIE3 strain indicated that BcPIE3 is dispensable for ergosterol biosynthesis. The systematic identification of EBD-containing proteins included in public databases showed that these proteins constitute a protein superfamily present only in eukaryotes. Phylogenetic analysis showed that the ancestral EBD-encoding gene was duplicated in the common ancestor of animals and fungi after the split from plants. Finally, we present evidence that the EBP phylogenetic clade of this superfamily has further expanded exclusively in euascomycetes, especially in *B. cinerea*, which contains three copies of the *EBP* gene.

Botrytis cinerea is a ubiquitous fungus capable of infecting a wide range of plants, fruits, and ornamentals at any stage of their development (15, 30). In order to identify novel pathogenicity determinants, we recently studied the expression profiles of *B. cinerea* genes during the infection of *Arabidopsis thaliana* leaves. Among the genes shown to be induced in planta, one called *B. cinerea PIE3* (Bc*PIE3*) was found to be highly expressed 24 to 29 h after the inoculation of the fungus onto the plant leaves (18). To gain insight into early infection events, this gene was further studied.

BcPIE3 showed strong similarity to mammalian emopamil binding proteins (EBPs). EBPs are integral, nonglycosylated proteins of the endoplasmic reticulum membrane, characterized by the presence of four transmembrane (TM) segments forming a binding domain for the drug emopamil, a phenylalkylamine Ca^{2+} antagonist. This domain is called the emopamil binding domain (EBD). Mammalian EBPs (43, 25) have received increasing attention due to their binding properties. Indeed, the binding of sigma ligands but also of numerous, structurally diverse drugs and fungicides on the EBD (36) exerts anti-ischemic effects in animal models (43). Mammalian EBPs have been further studied because of a number of syndromes caused by *EBP* gene mutations, such as the genetic disorder X-linked dominant chondrodysplasia punctata, Conradi-Hünermann syndrome (5, 26), CHILD (congenital hemidysplasia with ichthyosiform erythroderma and limb defects) syndrome (21), and the "tattered" mouse phenotype (13).

According to the above-mentioned studies, the molecular pathology of these syndromes is directly linked to alterations in the biochemical activity of EBPs, characterized as Δ^8-Δ^7 sterol isomerases (SIs) in mammals (52, 2) and plants (22). SIs (EC 5.3.3.5) act at one of the last steps of the postsqualene sterol biosynthesis pathway. Interestingly, the EBD is also present in another type of proteins, called EBP-like proteins, which have been identified in vertebrates (47). The only studied EBP-like protein, the human EBP-like protein, lacks both the SI and the sigma ligand binding activities, despite sharing basic structural features with EBPs. Its function is still unknown (47).

In this context, we investigated the relatedness of the BcPIE3 protein to human EBP and the EBP-like protein by amino acid sequence and secondary-structure comparisons. Furthermore, we analyzed the expression of the Bc*PIE3* gene at a prepenetration stage, as well as the virulence and the sterol content of a ΔBcPIE3 mutant, obtained by targeted inactivation of the gene in the wild-type strain T4 of *B. cinerea*. Moreover, we searched for sequences coding for the EBD in the *B. cinerea* genome and other released genomes. The phylogenetic analysis of the identified protein sequences revealed that EBD proteins (EBDPs) constitute a superfamily, which shows specific expansion within the euascomycete phylum. The phylogenetic relationships among eukaryotic EBDPs are discussed below.

* Corresponding author. Mailing address: UMR1290 BIOGER-CPP, INRA, Route de St-Cyr, 78026 Versailles, France. Phone: 33 (0) 1 30 83 32 10. Fax: 33 (0) 1 30 83 31 95. E-mail: natassa_g_2000@yahoo.com.

▽ Published ahead of print on 21 December 2007.

MATERIALS AND METHODS

Fungal strains, in vitro cultures, and pathogenicity assays. The wild-type *B. cinerea* strain T4 was isolated from infected tomato (40). Wild-type and mutant strains were maintained on solid-medium plates, and cultures in rich liquid

medium were performed as previously described (18). For sterol extractions, 10^8 spores were inoculated into 0.1 liter of rich medium. For in vitro preparations of *B. cinerea* appressoria, spore suspensions were grown for 10 h on 10-cm^2 Teflon filters with H_2O–0.4% agar as previously described (20). Pathogenicity assays of bean and tomato leaves were performed using fungal spore suspensions as previously described (57). These assays were repeated at least five times; each repetition comprised two independent measures of lesion size per strain.

Penetration assays and cytological studies. Assays of onion epidermis penetration were performed as previously described (20). For cytological studies, H_2O_2 in infected bean leaves was visually detected by using 3,3-diaminobenzidine (DAB) as a substrate (56). Leaves were vacuum infiltrated with a 1-mg/ml solution of DAB, pH 3.2, for 20 min. Air was extracted, and leaves were left on the DAB solution for 8 h under light at 25°C. A Leica MZ 16F stereomicroscope was used to observe the colored H_2O_2, and photographs at magnifications of ×1 and ×5 were taken with a Leica DC 300FX digital camera. Both penetration assays and DAB-staining experiments were repeated twice, with identical results from the repetitions.

Construction of *B. cinerea* Bc*PIE3*-disrupted mutants. For the disruption of the Bc*PIE3* gene, Seamless cloning kit (Stratagene) primers were used for the amplification of (i) the Bc*PIE3* cDNA (GenBank accession no. DQ140394) (primers SeamUp547, AGTTACTCTTCACACGCACAAGAAAAGCCAAGG ATG, and SeamLow488, AGTTACTCTTCATGGCTTGCGGAAGCCATAAC ACTG) from the pBSII SK^+ plasmid (Stratagene) and (ii) the bialaphos resistance gene *BAR* (primers *BAR*Up, TTACTCTTCACCACCTGAATGGGGAA TGGAAAT, and *BAR*Low, TTACTCTTCAGTGCACGGAAATGTTGAATA CTC) from the plasmid pCB1265 (53). EamI digestion, followed by the ligation of the two fragments, led to the construction of the pBcPIE3Δ vector, in which a 38-bp fragment of the cDNA beginning at bp 493 (corresponding to bp 656 following the ATG) was replaced by 1,000 bp of the selection marker gene *BAR* (Fig. 2). The pBcPIE3Δ insert was amplified by PCR with universal primers M13 and reverse-M13 and introduced into the genome of wild-type isolate T4 by using polyethylene glycol-mediated transformation of protoplasts (40). A hundred single-spore bialaphos-resistant transformants were isolated from the transformation and maintained as previously described (18). For the complementation of the Δ36 strain, we amplified by PCR (using the Phusion *Taq* polymerase Finnzymes) a 1,944-bp genomic fragment containing the Bc*PIE3* gene, including 409 bp of the 5′ untranslated region (UTR) and 546 bp of the 3′ UTR. We used primers that added SpeI and SacII restriction sites at the 5′ and 3′ extremities, respectively (UpSpeI, ATGACTAGTAAAGTCCGCACGTTAATTGG, and LowSacII, TTCCCGCGGGAGAAGCGCATCGGTAGTTC). The purified amplification product was digested with SpeI and SacII enzymes (Invitrogen) and cloned into the corresponding restriction sites of the pBSHygro plasmid (57), which contained the gene conferring resistance to hygromycin. The resulting vector, called p*BcPIE3*Hygro, was introduced into the genome of the Δ36 strain by using the same procedure of transformation. Fifteen single-spore hygromycin- and bialaphos-resistant transformants were isolated from this transformation.

Nucleic acid manipulations. RNA preparations and quantitative reverse transcription-PCR (qRT-PCR) experiments were performed as previously described (18); 4 μg of RNA coming from in vitro-prepared appressoria was subjected to reverse transcription. Amplifications of 101 bp of the Bc*PIE3* and 110 bp of the Bc*PLS1* transcripts were made using primers Bc*PIE3*Up (CCGGAACCATTG TACTTTTGG) and Bc*PIE3*Low (CTTGCGGAAGCCATAACACT) and AS23 (CGTCCTACTATTGCCAGTGT) and AS32 (GGAATGGAGATGAGGAAG GC), respectively. For Southern blotting experiments, genomic DNA was extracted from 2-day-old mycelia by using the Sarkosyl extraction method as previously described (12). The DNA was digested with the SacII enzyme by using standard procedures (50) and probed with the p*BcPIE3*Hygro plasmid vector.

Sterol quantifications and growth inhibition tests. The isolation and identification of total unsaponifiable lipids were performed as follows. The lyophilized mycelium sample (300 mg), coming from 2-day-old cultures in rich medium, was saponified in methanolic KOH (60 g $liter^{-1}$) at 70°C for 2 h. Unsaponifiable lipids were extracted into hexane three times and then purified on silica gel thin-layer chromatography (TLC) plates, as described elsewhere (11). Dichloromethane was used as the developing solvent (two runs), and the steryl compounds were visualized under UV light (366 nm), after spraying of the TLC plates with a 0.1% solution of berberine hydrochloride in ethanol. The 4,4-dimethyl-, 4α-methyl-, and 4-desmethylsterol fractions migrated at retention factor (Rf) values of 0.56, 0.47, and 0.38, respectively (see Table 1). The silica gel containing these bands was scraped off and eluted with dichloromethane. The 4,4-dimethyl-, 4α-methyl-, and 4-desmethylsterol fractions were acetylated at room temperature for 15 h by using a mixture of pyridine and acetic anhydride (ratio of 1:2, vol/vol). The steryl acetates were then analyzed by gas chromatography (GC) and GC-mass spectrometry (MS). The GC was fitted with a flame ionization detector and an XTI-5 capillary column (30 m by 0.32 mm), with helium at 9,104 Pa. The oven temperature was 290°C. Cholesterol was used as the standard for relative retention time (RRT) determination and the quantification of steryl compounds. GC-MS analyses were performed with a Ribermag R10-10-C spectrometer. The ionization potential was 70 eV. The components of the fractions were identified from their RRTs and mass spectra.

Drug sensitivity assays of *B. cinerea* conidia for germ tube elongation measures and of mycelia for radial growth measures were conducted as previously described (38). Fungal development was monitored over 24 h and 3 to 6 days, respectively. These experiments were repeated at least three times; each repetition comprised two independent assays per strain.

Identification and phylogenetic analysis of EBDPs. tBlastn queries, with two iterations, of the NCBI, the Broad Institute, and the Genolevures (http://cbi.labri.fr/Genolevures/) databases were performed using the BcPIE3 protein sequence as a template. The E value cutoff used for the retention of significant hits was 10^{-18}. Only genomes with coverage of at least 10-fold were kept for analysis, to avoid incomplete-genome-derived biases. As an exception, we included the genome of *Sclerotinia sclerotiorum*, with sevenfold coverage, because this fungus is closely related to *B. cinerea* (Sclerotiniaceae family). As there were multiple hits in some genomes, the existence of distinct proteins was verified by pairwise alignments among protein sequences corresponding to the same genome (species) and chromosome/supercontig positioning, when this information was available. Automatic gene annotations were improved manually for seven genes, one of which was not predicted by automatic software Blastx alignment data; FGenesh (http://www.softberry.com) and GeneWise (4) automatic predictions were used for these annotation tasks. Newly determined sequences coded for proteins designated Bcinerea2, Bcinerea4, Anidulans2, Anidulans3, Fgramine1, Fgramine2, and Mgrisea2 in the phylogenetic tree (see Fig. 6).

Full-length EBDPs from vertebrates, plants, and fungi were manually aligned with BioEdit 5.0.9 (24). The phylogeny of EBDPs was inferred by maximum likelihood, and the tree reconstruction was completed using PHYML (23) with the Jones-Taylor-Thornton model of protein evolution (32), the BIONJ tree as the initial tree, and 500 bootstrap replicates. The discrete gamma model was used to account for variable substitution rates among sites, with four different categories of substitution rates; the gamma distribution parameter, estimated from the data, was 1.21, indicating moderate variation of substitution rates among sites. The proportion of invariable sites was also estimated from the data and was 0.062. For this analysis, ambiguous positions containing gaps were removed from the alignment. We also performed an unweighted maximum-parsimony analysis using PAUP 4.0 software (54) with a heuristic search (tree bisection-reconnection branch swapping; maximum number of trees, 5,000) and 500 bootstrap replicates (simple stepwise addition), as well as distance reconstruction using the PROTDIST program implemented in the PHYLIP package, version 3.6a3 (16), with the Dayhoff point accepted mutation (PAM) matrix as a distance model and the neighbor-joining algorithm for tree reconstruction. Topologies recovered by parsimony with different coding residues for gaps (positions considered to be either missing or filled by stuffer amino acids or assigned a weight of 1 for a gap's opening but no weight for a gap's elongation) were not significantly different from one another (data not shown).

For the definition of consensus motifs, the alignment of 42 EBDPs was examined; we noted as X the positions for which more than three possibilities of amino acids were available.

Nucleotide sequence accession numbers. The newly determined sequences were submitted to the GenBank database under the following accession numbers: Bc*EBDP2*, EF173622; Bc*EBDP4*, EF173620; *Aspergillus nidulans EBDP2*, EF173623; *Aspergillus nidulans EBDP3*, EF173625; *Fusarium graminearum EBDP1*, EF173624; *Fusarium graminearum EBDP2*, EF173620; and *Magnaporthe grisea EBDP2*, EF173626.

RESULTS

The Bc*PIE3* gene shows maximal expression at the early infection stage. In a previous study, the Bc*PIE3* gene was shown to be up-regulated in the early stage of *Arabidopsis thaliana* leaf infections with the *B. cinerea* T4 strain (18). Here, we undertook qRT-PCR analysis of cDNAs synthesized from RNA extracted from appressoria of strain T4. The tetraspanin gene Bc*PLS1* (19) was used as a reference, as the BcPLS1 protein is required for appressorium-mediated penetration (20). A gene down-regulated in planta and a gene up-regulated

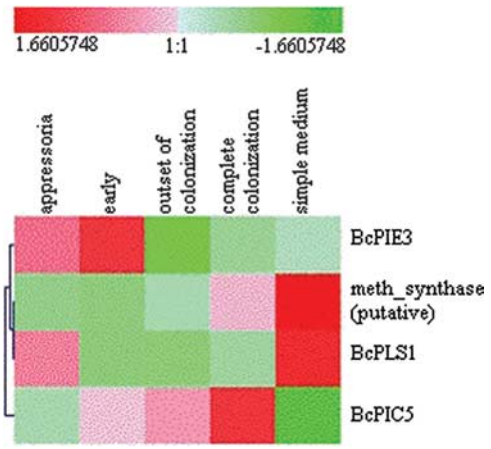

FIG. 1. Expression profile of Bc*PIE3* gene. The graphic represents changes in cycle threshold expression values obtained from qRT-PCR and submitted to average linkage hierarchical clustering. Changes in cycle threshold expression values were normalized with the mean expression value for two constitutive genes and transformed to $\log_2$ prior to clustering. Conditions tested (columns) were as follows: stage of appressorium formation on Teflon filters (see Materials and Methods), three consecutive stages of *Botrytis* in planta growth on *Arabidopsis* leaves (early stage, outset of colonization, and complete-colonization stage), and one stage of in vitro growth on a simple medium. These stages, the RNA preparation method, and identities of constitutive genes have been detailed by Gioti et al. (18). Apart from Bc*PIE3*, additional genes (rows) presented here as controls code for a putative methionine synthase (meth_synthase; AL14398), down-regulated in planta; a fungal tetraspanin named BcPLS1, specifically expressed in appressoria; and an FKBP12 protein, up-regulated in planta at the complete-colonization stage (18).

at a late stage of infection of *Arabidopsis thaliana* leaves (18) served as additional controls. The qRT-PCR expression profiles of Bc*PIE3* and Bc*PLS1* during the appressorium formation stage, as well as during in vitro growth (mycelial growth in simple medium) and the in planta progression of *B. cinerea* are illustrated in Fig. 1. Bc*PLS1* exhibited high expression levels during the appressorium formation stage and almost undetectable expression levels during the infection of *Arabidopsis thaliana* leaves. Bc*PIE3* was highly expressed during appressorium formation, with its expression level reaching its maximum at the early stage of infection (18) and then decreasing gradually beyond the level of expression in vitro.

Disruption of Bc*PIE3* gene in T4 wild-type strain. Bc*PIE3* is present as a single copy in the genome of the wild-type strain T4 (http://www.cns.fr/externe/Francais/Projets/Projet_LN/organisme_LN.html). Its disruption (Fig. 2A) was carried out using a partial cDNA sequence (GenBank accession no. DQ140394). First, we constructed a plasmid vector (pBcPIE3Δ) in which this cDNA was interrupted after nucleotide 493 by the *BAR* gene, conferring resistance to bialaphos (Fig. 2A). The amplified insert of the pBcPIE3Δ plasmid was used to transform protoplasts of *B. cinerea* strain T4. From a total of 100 purified transformants screened by PCR (data not shown), one disruption mutant, called Δ36, was obtained (Fig. 2B). For complementation, a plasmid containing the Bc*PIE3* gene upstream of the hygromycin resistance gene (p*BcPIE3*Hygro) was introduced by transformation into the genome of the Δ36 strain with the same procedure. From 15 transformants obtained, one mutant, called cp12, was retained as it contained a single ectopic integration of the Bc*PIE3* locus.

Disruption of Bc*PIE3* affects virulence. The Δ36 mutant showed sporulation and growth rates similar to those of the wild-type strain and the complemented mutant cp12 on plates with rich solid medium (data not shown). The virulence of inactivated and complemented mutants on detached bean and tomato leaves was assessed. On bean leaves, primary lesions appeared at 3 days postinoculation (dpi) with spore suspensions. At this stage, the diameters of the lesions caused by all

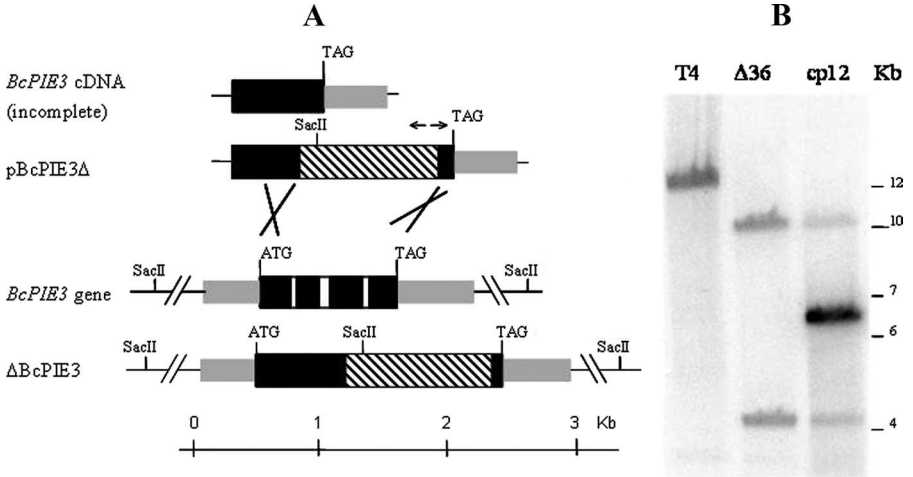

FIG. 2. Disruption of Bc*PIE3* gene. (A) Strategy for disruption. The Bc*PIE3* gene was interrupted using Seamless technology with a partial cDNA sequence from the T4 strain. Gray boxes represent 5′ and 3′ UTRs, and black boxes represent exons. The stop codon (TAG) was located 453 bp upstream of the 3′ end of the cDNA. For the construction of the pBcPIE3Δ vector, the Bc*PIE3* cDNA, except for 38 bp after the 493rd base, was amplified (arrows), and the 38-bp fragment was replaced by the selection marker gene *BAR* (white box). The insert of pBcPIE3Δ was amplified before the transformation of wild-type T4 protoplasts. During transformation, homologous recombination with the genomic Bc*PIE3* sequence (thick lines) gave the ΔBcPIE3 disrupted mutant Δ36. Note that the start codon (ATG) was located 163 nucleotides upstream from the partial cDNA sequence used for disruption. (B) Southern blot representing the molecular patterns of wild-type T4, inactivated mutant Δ36, and the cp12 restored mutant. Genomic DNA was digested with the SacII enzyme and probed with the p*BcPIE3*Hygro plasmid.

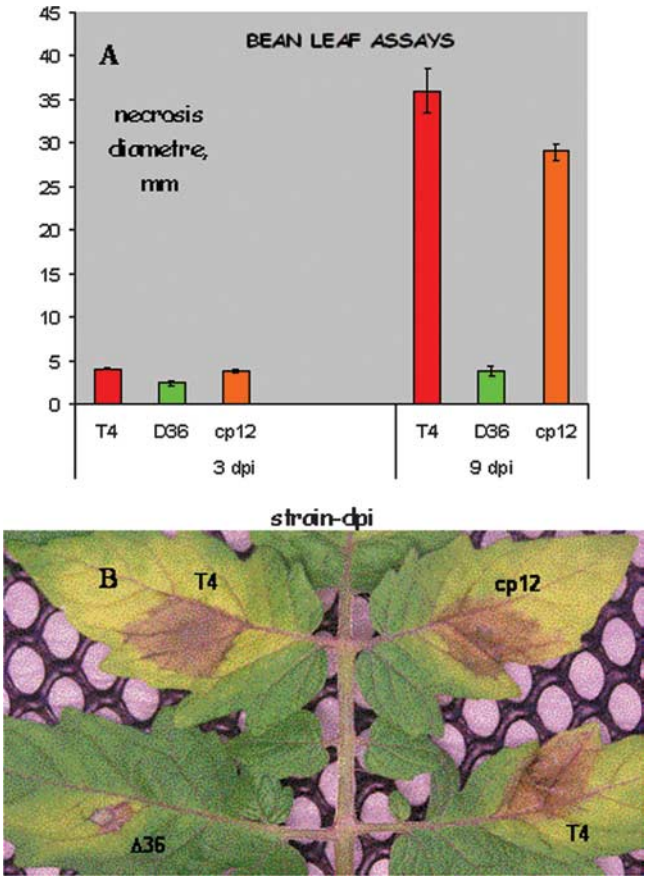

FIG. 3. Pathogenicity assays with the Δ36 strain. (A) Histogram representing the correlation of the diameters of the lesions caused by the wild-type T4, inactivated mutant Δ36, and restored cp12 mutant strains at 3 and 9 dpi with fungal spores. Assays were conducted with detached bean leaves carrying droplets containing 1,000 spores of the fungus in a 10 mM NaH_2PO_4–10 mM glucose solution. (B) Infected tomato leaves at 5 dpi. The lesions caused by the Δ36 strain were blocked, in contrast to those caused by the wild-type strain T4 and the complemented mutant cp12, which invaded the leaf.

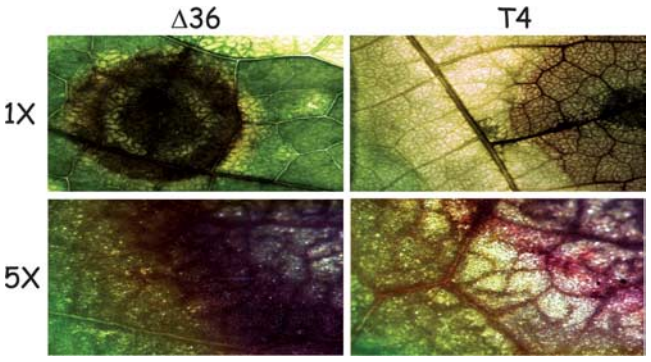

FIG. 4. In planta cytological study of the mutant Δ36. Microscopic view of the fungus-plant interface at 5 dpi with 10^4 fungal spores. DAB staining allows the visualization of hydrogen peroxide (dark brown). The mutant Δ36 strain (left) and the wild-type T4 strain (right) were compared at actual size (upper panels) and at a magnification of ×5.

strains (Δ36, 2.5 ± 1.41 mm; T4, 4.11 ± 1.15 mm; cp12, 3.8 ± 1 mm) did not exhibit any statistically significant differences (Fig. 3A). The outgrowth of lesions caused by the Δ36 strain was strongly reduced from this point on, reaching only 3.89 ± 2.85 mm at 9 dpi, while T4 and cp12 lesions reached 36 ± 15.21 and 29 ± 5 mm, respectively (Fig. 3A). Thus, lesion diameters in infections caused by the Δ36 mutant were reduced by 89% compared to those in infections caused by the wild type T4. On tomato leaves, the formation of primary necrotic lesions occurred 1 day earlier than that on bean leaves, but the outgrowth of lesions caused by the Δ36 mutant was reduced to a degree similar to that of lesions on bean leaves (lesion diameter at 7 dpi, 11 ± 6 mm, as opposed to 42 ± 9 mm for T4 lesions and 38 ± 5 mm for cp12 lesions). Lesion diameters in tomato infections caused by the Δ36 strain were thus reduced by 74% compared to those in infections caused by the wild type T4. Moreover, similar to those in bean leaf infections, the lesions caused by the Δ36 mutant failed to completely invade the leaf (Fig. 3B).

Given that the reduction in virulence of the Δ36 mutant could not be attributed to a general impairment in growth, we then investigated whether this mutant was deficient in a process directly linked to in planta development. To this end, germinating spores of strains T4 and Δ36 were observed under the microscope to investigate their ability to form penetrating appressoria on onion epidermis. During these experiments, both strains penetrated successfully; no significant differences concerning their penetration rates or efficacy were observed (data not shown). We then compared H_2O_2 accumulation levels during the infections caused by the wild-type strain T4 and the mutant strain Δ36. Pathogenicity assays of the two strains on bean leaves were performed, and H_2O_2 DAB staining was performed for the time period between days 2 and 5 postinoculation. These time points cover the period when the phenotype of the Δ36 strain is apparent. Interestingly, in contrast to the T4 wild-type stain, the Δ36 strain was not able to expand beyond the limit of the brown-stained H_2O_2 area after the third day of infection (Fig. 4).

Disruption of Bc*PIE3* does not affect sterol content or fungicide/pharmacophore-mediated toxicity. We investigated whether the BcPIE3 protein is involved in the biosynthesis of ergosterol, the main sterol in most yeast species, such as *Saccharomyces cerevisiae*, and fungi (58). To this end, the sterol profiles of unsaponifiable mycelium fractions extracted from 2-day cultures of T4 and Δ36 strains were analyzed by TLC, GC, and MS. The T4 wild-type strain amounts of 4-desmethylsterols, 4α-methylsterols, and 4,4-dimethylsterols (Table 1) were similar to those reported previously for other *B. cinerea* wild-type strains (11). The sterol profile of the Δ36 strain did not show any significant variation compared to that of T4 concerning the total or individual levels of sterol compounds (Table 1).

We next examined the growth of wild-type T4 and the Δ36 mutant in the presence of fungicides and drugs known to mediate growth inhibition via binding to the yeast and mammalian SIs ERG2 (ergosterol biosynthesis gene 2) and EBP, respectively (45, 44, 36). Germ tube elongation and mycelial growth on rich-medium plates containing haloperidol, trifluoperazine, and amiodarone and the fungicides tridemorph, piperalin, fenpropimorph, and fenpropidin, respectively, were monitored. Tridemorph and piperalin inhibit mainly the Δ^8-Δ^7 isomerase activity in fungi (51, 9, 10), whereas fenpropimorph and fenpropidin inhibit mainly the Δ^{14} reductase activity but can also

TABLE 1. Chromatographic properties and contents of unsaponifiable lipids of *B. cinerea* strain T4 and disruption mutant Δ36[a]

Unsaponifiable lipid	TLC Rf	GC RRT	Sterol composition (% of total sterol)	
			T4	Δ36
Sterols				
4-Desmethylsterols	0.38			
Lichesterol		1.31	14.2	9.0
Ergosterol		1.38	80.2	82.1
Ergosta-7,22-dien-3β-ol		1.42	0.9	1.6
Fecosterol		1.47	0.5	0.8
Ergosta-5,7,24(24[1])-trien-3β-ol		1.51		
Ergosta-5,7-dien-3β-ol		1.52	1.2	1.5
Episterol		1.56	1.6	3.3
4α-Methylsterol	0.47			
4α-Methylfecosterol		1.62	0.2	0.4
4,4-Dimethylsterols	0.56			
Lanosterol		1.62	0.2	0.1
Eburicol		1.79	0.6	0.7
4,4-Dimethylfecosterol		1.85	0.2	0.4
Other steryl compounds			0.2	0.1

[a] Rf values from TLC were measured with CH_2Cl_2 as the developing solvent (two runs). For the three main classes of sterols (4-desmethylsterols, 4α-methylsterols, and 4,4-dimethylsterols), composition values are expressed as percentages of total steryl compounds. The sums of unidentified and minor steryl compounds (occurring at an amount below 0.1) are noted as "other." RRTs for steryl acetates in GC experiments were expressed relative to cholesterol. The sterol composition was determined as 2.8 μg mg^{-1} (dry wt) and 3.3 μg mg^{-1} (dry wt) for T4 and Δ36 strains, respectively. These experiments were performed twice, with no significant variation in results.

TABLE 2. Effects of fungicides and drugs on *B. cinerea* wild-type strain T4 and the Δ36 mutant[a]

Toxicant	EC_{50} (mg/liter) for mycelium growth of strain:		EC_{50} (mg/liter) for filament elongation of strain:	
	T4	Δ36	T4	Δ36
Tridemorph	0.20	0.30	0.020	0.015
Fenpropimorph	0.15	0.20	0.015	0.020
Fenpropidin	0.35	0.40	0.050	0.060
Piperalin	10	8	2	1
Haloperidol	>25	>25	13	10
Triflupiperazine	15	18	6	3
Amiodarone	8	8	4	4

[a] These effects are expressed as 50% effective concentrations (EC_{50}s), i.e., the concentrations causing 50% reduction in germ tube elongation and mycelium radial growth.

act on the Δ^8-Δ^7 isomerase in some fungi (8, 9, 10). Among the drugs tested in an indirect assessment of binding to the EBD, amiodarone was the most structurally related to emopamil (36). In the presence of all the above-named toxicants, the growth of the wild-type strain T4 was inhibited, as previously reported for other *B. cinerea* wild-type field isolates (38). No significant difference in fungal development between T4 and the Δ36 mutant was observed, either in evaluations with the above-mentioned toxicants (Table 2) or in tests with fungicides inhibiting other enzymes of the ergosterol biosynthesis pathway (data not shown).

BcPIE3 protein features. The Bc*PIE3* gene has three introns and encodes a 274-amino-acid protein (Broad Institute protein identification no. BCIG_13631.1) with an estimated molecular mass of 31 kDa. A BlastP search of the Conserved Domain Database (42) using the BcPIE3 amino acid sequence as a template allowed the identification of an EBD ranging between amino acid positions 33 and 214 (E value of alignment, 7e−33). We further investigated the relatedness of BcPIE3 to two human proteins containing this domain, the EBP and the EBP-like protein, by full-length sequence alignments. BcPIE3 showed 38% identity and 53% similarity to the human EBP and 29% identity and 47% similarity to the human EBP-like protein.

We then focused on the conservation of amino acid residues important for the biochemical functions of EBP. Moebius and colleagues (46) had previously identified 11 amino acids in the human EBP which are critical for Δ^8-Δ^7 sterol isomerization. Directed mutations in these residues cause 90 to 100% reduction in the sterols produced (Fig. 5). Six of these residues have been noted to be required for isomerization, and five have been noted to be functionally important. All of them were found to be conserved in BcPIE3. Another feature common among the human EBP and EBP-like protein and BcPIE3 is the high percentages of aromatic amino acids in the TM domains (23% in EBP and BcPIE3 and 18% in the EBP-like protein). This is a characteristic feature of both broad-substrate-specificity transporters (48) and enzymes with activities that imply the stabilization of carbocations, such as the Δ^8-Δ^7 isomerase (49, 47).

The C-terminal sequence motifs KK and KXK in positions −3 and −4 and −3 to −5, respectively, were previously proposed to constitute endoplasmic reticulum retention motifs (3, 28). These motifs were detected in all three proteins, but in BcPIE3 the requirement for their position was not fulfilled (Fig. 4). BcPIE3 protein was predicted to locate at the endoplasmic reticulum membrane according to Protcomp version 6.0 software (http://www.softberry.com). The latest orientation model for the human EBP showed that the protein localizes in the lumen of the nuclear envelope, a specialized subcompartment of the endoplasmic reticulum consisting of inner and outer membranes, nuclear pore complexes, and nuclear lamina (14). BcPIE3 was also predicted to localize in this compartment according to the SVM software (37).

The hydrophobic profiles of the three proteins were analyzed by standard prediction algorithms TMPred (27) and Kyte-Doolittle (35) and by hydrophobic cluster analysis (HCA), permitting the visualization of secondary structures (17, 59). In these analyses, the three proteins showed significant conservation (Fig. 5): BcPIE3, the human EBP, and the human EBP-like protein have five predicted TM domains and a central loop between the second and third TM domains. This loop is characterized by the presence of a putative β-sheet and an α-helix, and the α-helix in each protein contained the same amino acid sequence, WKEY. Moreover, similar secondary structures were detected at the same relative positions in the three proteins (Fig. 5): (i) a mosaic cluster and an α-helix at the N terminus; (ii) a putative β-sheet between TM domains 1 and 2, clearly visible in the EBP-like protein and present in the

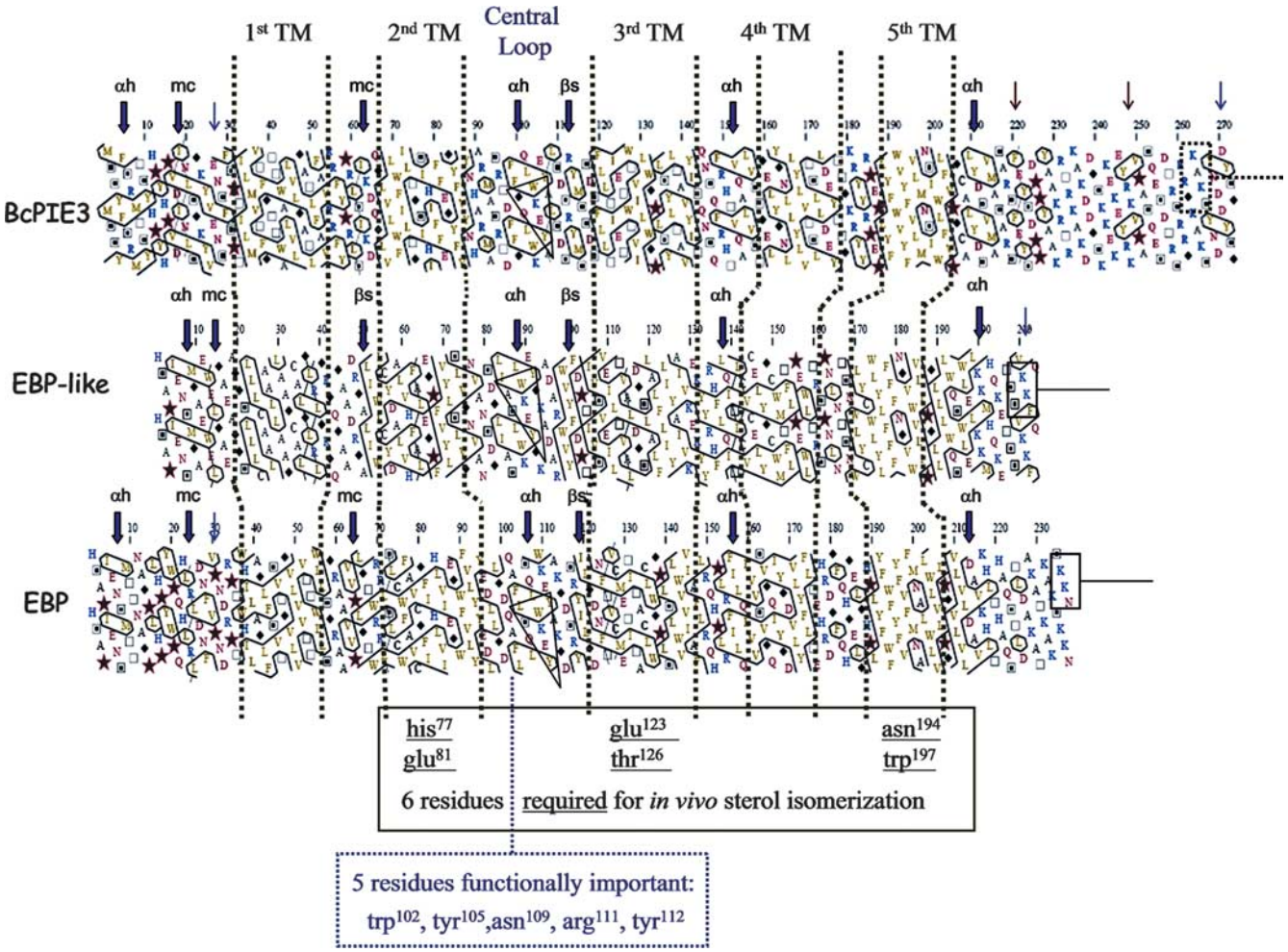

FIG. 5. Secondary-structure comparison (HCA) between the BcPIE3 protein and the human EBP and EBP-like protein. In these plots, the protein sequences are written on a duplicated α-helical net and the contours of hydrophobic clusters are automatically drawn (boxed). The standard one-letter code for amino acids is used, except for proline, glycine, threonine, and serine, which are represented by stars, diamonds, squares, and squares with a dot, respectively. The positions of TMs are marked with dotted lines. The region between the second and the third TM corresponds to the central loop. The most important hydrophobic clusters (αh, α-helix; βs, β-sheet; and mc, mosaic cluster) are marked with arrows. Thick blue arrows are used for clusters that are common among the three proteins, thin blue arrows are used for those common between only two proteins, and thin red arrows are used for those found exclusively in one protein. Note that clusters were considered to be groups comprising at least two hydrophobic residues present in at least two of the proteins studied here. The triangle in the central loop region shows the conserved sequence WKEY. Positions of residues which are functionally important or required for in vivo sterol isomerization (46) are illustrated in the amino acid sequence of the human EBP. All of them are present in BcPIE3 and the EBP-like protein, except Tyr^{112}, which is absent from the EBP-like protein. The endoplasmic reticulum retrieval motif KXK/KK (positions −3 to −5/−3 and −4) in the N-terminal regions of the EBP and the EBP-like protein is shown. We noted the same motif in the BcPIE3 N terminus, although the positioning requirement of −3 to −5/−3 and −4 was not fulfilled.

form of a mosaic cluster in the other two proteins (indeed, mosaic clusters are often associated with β-sheets [7]); (iii) an α-helix between TM domains 3 and 4; and (iv) an α-helix at the C-terminal region. This C-terminal region was notably the most divergent among the three proteins (Fig. 5).

Identification and phylogenetic analysis of eukaryotic EBDPs. In order to obtain an exhaustive data set of EBDPs to which BcPIE3 showed significant similarity, tBlastn iterative queries of public databases were performed. This research resulted in the identification of 42 EBDPs from 22 species: 13 fungi (9 euascomycete and 4 basidiomycete species), 6 vertebrates, and 3 plants. No EBD-encoding gene was found in hemiascomycete, invertebrate, or prokaryotic genomes. In euascomycetes, four EBD-encoding genes were found in the genome of *B. cinerea*, three were found in each of the genomes of *Sclerotinia sclerotiorum*, *Aspergillus fumigatus*, *Aspergillus nidulans*, *Aspergillus oryzae*, *Fusarium graminearum*, and *Magnaporthe grisea*, and two were found in each of the genomes of *Neurospora crassa* and *Stagonospora nodorum*. Two EBD-encoding genes in each of the vertebrate genomes were also identified, as previously reported (47). Finally, a single EBD-encoding gene was detected in the genomes of the basidiomycete species *Ustilago maydis*, *Phanerochaete chrysosporium*, *Coprinus cinereus*, and *Laccaria bicolor* and of the plants *Arabidopsis thaliana*, *Zea mays*, and *Oryza sativa*.

In order to explore the phylogenetic relationships among

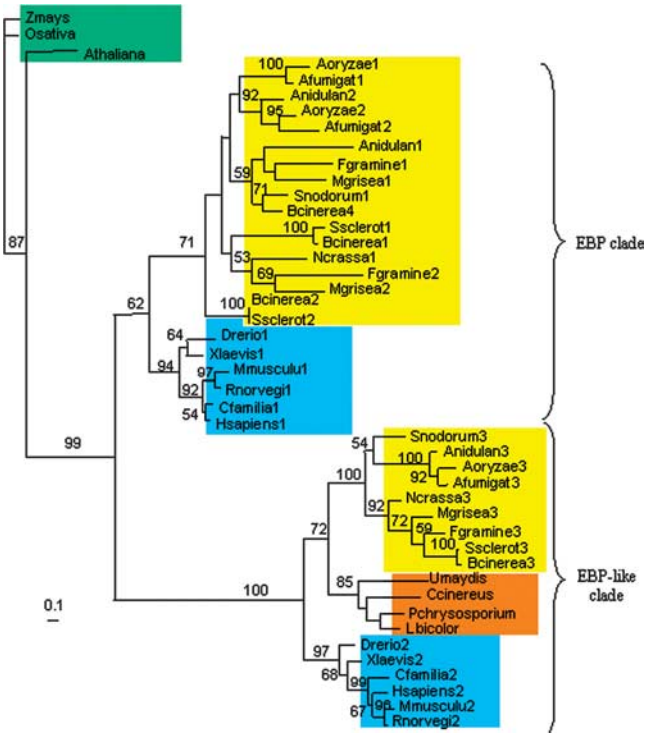

FIG. 6. Phylogenetic analysis of eukaryotic EBDPs. The tree was reconstructed with the maximum-likelihood method. Numbers located in the nodes indicate bootstrap values. EBDPs from plants (*Oryza sativa*, accession no. XP_462727.1; *Arabidopsis thaliana*, accession no. AAD04752; and *Zea mays*, accession no. AAT02417) were treated as an out-group. They are noted in green, whereas vertebrate EBDPs are noted in blue and fungal EBDPs are noted in yellow, except those from basidiomycete species, noted in orange. Fungal EBDPs clustering together with the vertebrate EBP-like proteins designated by the species name followed by the number 2 (Drerio2 [from *Danio rerio*], accession no. XP_692880; Xlaevis2 [from *Xenopus laevis*], accession no. AAH78134; Cfamilia2 [from *Canis familiaris*], accession no. XP_534113; Hsapiens2 [from *Homo sapiens*], accession no. NP_115954, Mmusculu2 [from *Mus musculus*], accession no. AAK28349; and Rnorvegi2 [from *Rattus norvegicus*], accession no. XP_341335) were all designated by the species name followed by the number 3 (Snodorum3 [from *Stagonospora nodorum*], accession no. EAT79604; Anidulan3 [from *Aspergillus nidulans*], accession no. XP_868878, Aoryzae3 [from *Aspergillus oryzae*], accession no. BAE59668; Afumigat3 [from *Aspergillus fumigatus*], accession no. XP_755724; Ncrassa3 [from *Neurospora crassa*], accession no. XP_961099; Mgrisea3 [from *Magnaporthe grisea*], accession no. XP_368532; Fgramine3 [from *Fusarium graminearum*], accession no. XP_387327; Ssclerot3 [from *Sclerotinia sclerotiorum*], accession no. SS1G_00037.1; and Bcinerea3 [from *B. cinerea*], accession no. BC1G_11686.1), except for those from basidiomycete species, which possess only one EBDP (Umaydis [from *Ustilago maydis*], accession no. XP_761356; Ccinereus [from *Coprinus cinereus*], accession no. EAU85829; Pchrysosporium [from *Phanerochaete chrysosporium*], accession no. Scaffold 54:10-984; and Lbicolor [from *Laccaria bicolor*], accession no. 322659-fgenesh3_pg.C_scaffold_3000276). Fungal EBDPs clustering together with the vertebrate EBPs designated by the species name followed by the number 1 (Drerio1 [from *Danio rerio*], accession no. NP_001002328; Xlaevis1 [from *Xenopus laevis*], accession no. AAH55967; Mmusculu1 [from *Mus musculus*], accession no. AAH04703; Rnorvegi1 [from *Rattus norvegicus*], accession no. AAQ14592; Cfamilia1 [from *Canis familiaris*], accession no. XP_851024; and Hsapiens1 [from *Homo sapiens*], accession no. AAH01549) were designated by the species name followed by the numbers 1 to 4 (Aoryzae1, accession no. BAE59581, and Aoryzae2, accession no. BAE56166 [both from *Aspergillus oryzae*]; Afumigat1, accession no. EAL86364, and Afumigat2, accession no. EAL90841 [both from *Aspergillus fumigatus*], Anidulan1, accession no. XP_680480, and Anidulan2, accession no. EF173623 [both from *Aspergillus nidulans*]; Fgramine1, accession no. EF173624, and Fgramine2, accession no. EF173620 [both from *Fusarium graminearum*]; Mgrisea1, accession no. XP_362129, and Mgrisea2, accession no. EF173626 [both from *Magnaporthe grisea*]; Ncrassa1 [from *Neurospora crassa*], accession no. XP_957817; Snodorum1 [from *Stagonospora nodorum*], accession no. EAT90433.1; Bcinerea1 [BcPIE3], accession no. DQ140394, Bcinerea2, accession no. EF173622, and Bcinerea4, accession no. EF173620 [all from *B. cinerea*]; and Ssclerot1, accession no. SS1G_07733.1, and Ssclerot2, accession no. SS1G_06945.1 [both from *Scleotinia sclerotiorum*]). Protein identities came from the NCBI database, except those for *Laccaria bicolor* and *Phanerochaete chrysosporium* (http://genome.jgi-psf.org/) and *Scleotinia sclerotiorum*, *Stagonospora nodorum*, and *B. cinerea* (http://www.broad.mit.edu/annotation/fungi/).

eukaryotic EBDPs, their full-length amino acid sequences were aligned and the resulting multiple alignment was submitted to different phylogram reconstruction methods using plant EBDPs as an out-group. Two distinct monophyletic clades were resolved regardless of the method used, whether maximum likelihood (Fig. 6) or distance or maximum parsimony (data not shown). The maximum-likelihood analysis resulted in a phylogenetic tree (likelihood [loglk] = −8,412.1) comprising two clades. In the first, strongly supported clade (bootstrap value = 100; 500 iterations), EBDPs encoded by single gene copies per fungal genome clustered together with vertebrate EBP-like proteins. This clade was named EBP-like, after the name of the only characterized protein of this group, the human EBP-like protein (47). Within this EBP-like clade, vertebrate and fungal proteins formed two monophyletic lineages (bootstrap values, 87 and 72, respectively). The fungal lineage was further divided in two clusters encompassing the EBP-like proteins encoded by single gene copies from the six euascomycete genomes and the four basidiomycete genomes (bootstrap values, 100 and 86, respectively).

The second clade grouped the remaining fungal EBDPs—encoded by gene copies numbering from one to three, depending on the species–together with vertebrate EBPs (bootstrap value = 82; 500 replicates). This clade was designated the EBP clade, after the human EBP (43). The EBP clade was divided into a highly supported monophyletic lineage formed by vertebrate EBPs (bootstrap value = 84) and a second monophyletic lineage containing euascomycete EBPs (bootstrap value = 71). According to preliminary analyses, the plant EBDPs (treated here as an out-group) were more closely related to the EBP clade.

DISCUSSION

BcPIE3 is a virulence factor required for lesion expansion. The gene Bc*PIE3* was a good candidate for a *B. cinerea* virulence determinant, due to its expression profile in planta, revealed by previous results from both macroarray and qRT-PCR experiments (18) and by in vitro appressorium formation in qRT-PCR experiments in this study. The virulence of the Δ36 mutant was severely reduced compared to that of the wild-type strain T4 (Fig. 3). At 7 dpi of fungal spores, the sizes of lesions caused by the Δ36 strain were reduced by 74% on tomato leaves and 89% on bean leaves compared to those caused by T4. Furthermore, complementation of the Δ36 mutant restored virulence to wild-type levels, confirming that the

observed reduction in the virulence of the mutant was due to the disruption of the Bc*PIE3* gene (Fig. 3).

BcPIE3 protein participates in the infection process via a yet-unidentified function. Even though the Bc*PIE3* gene was strongly expressed at the stage of appressorium formation (Fig. 1), the protein was not related to host penetration, as the mutant penetrated plant tissues normally (data not shown). BcPIE3 protein did not affect the appearance of primary lesions, but its activity was critical for their expansion, since the primary lesions caused by Δ36 failed to fully invade the leaf (Fig. 3B). The reduced ability of the mutant to grow through the reactive oxygen species (ROS)-rich region, at the necrotic-zone edge, further corroborates the hypothesis that the activity of BcPIE3 protein affects the ability of the pathogen to expand in the plant tissues. The mutant seemed, indeed, to be unable to cope with ROS, and this behavior may represent a plant defense reaction. However, more experiments are needed to establish whether the ROS detected in this study originated from the plant or the fungus.

It is noteworthy that the Bc*PIE3* gene shows maximal expression at the early stage of infection, that is, 24 to 29 h postinoculation (18), whereas the mutant's phenotype is apparent during the expansion of necrotic lesions. This stage, previously defined as the outset of colonization, occurs at 33 to 48 h postinoculation (18). These data suggest that the BcPIE3 protein may be fully functional or required only 9 to 19 h after the stage of the gene's maximal expression. This result will be useful for future protein purification experiments with BcPIE3.

Another issue to address in the future is the complete inactivation of the gene. In our experiments, the insertion of the *BAR* gene for Bc*PIE3* inactivation occurred after the position corresponding to the 218th predicted amino acid (Fig. 2A). This area encodes the C-terminal region after the last TM domain (Fig. 5). Considering this insertion position, it is likely that the Δ36 strain expressed a truncated form of BcPIE3 protein and that the reduced pathogenicity of Δ36 was linked to the problematic maturation and/or localization of the protein rather than its sensu stricto enzymatic or other activity. The generation of a new mutant in which the entire open reading frame has been deleted will permit the confirmation of this hypothesis.

A *B. cinerea* EBDP. BcPIE3 was compared with the human EBP and the EBP-like protein at the primary- as well as the secondary-structure level by HCA (17, 59). A three-dimensional structure of EBDPs is, however, unavailable, due to the high hydrophobicity of the EBD, which renders its crystallization a challenging task. These comparisons indicated that the three proteins not only show significant global similarity (47 to 53%) but also have conserved specific features, which are suspected or have been shown to play a role in their activity: the high percentages of aromatic amino acids in the TM regions and the 11 amino acid residues defined to be critical for the catalytic activity of the human EBP (46). Moreover, the comparison of HCA graphical predictions showed that the hydrophobic profile of BcPIE3 is very similar to the profiles of the human EBP and the EBP-like protein, notably considering the five TM domains and the central loop, as well as the distribution of secondary structures throughout the protein backbone (Fig. 5). Overall, protein alignments and predicted structure comparisons showed that the human EBP, the human EBP-like protein, and the newly identified BcPIE3 protein share hallmark features of the EBD. BcPIE3 is thus the first characterized EBDP in fungi.

BcPIE3 is dispensable for previously reported functions of EBP (ergosterol biosynthesis and ligand binding). All residues in the human EBP essential for SI activity (46) are conserved in BcPIE3 (Fig. 5). Phylogenetic analysis further showed that BcPIE3 belongs to the EBP clade (Fig. 6), whereas bidirectional best-hit BLAST searching (55) indicated that among *B. cinerea* EBPs, BcPIE3 is the most probable ortholog of the human EBP SI. However, several lines of evidence indicate that it does not play the same role as the human EBP:

First, BcPIE3 protein is dispensable for the biosynthesis of ergosterol, the end product of the biosynthetic pathway and the main sterol in most yeast and fungi. (i) The Δ36 mutant does not accumulate fecosterol or other Δ^8 sterols and produces levels of ergosterol similar to those produced by the wild type T4 under standard conditions (Table 1). (ii) The Δ36 mutant grows similarly to the wild type on standard-medium plates (data not shown). Ergosterol is an essential structural element of the cell membranes, as well as a regulatory component (58). Therefore, an ergosterol-deficient mutant would be expected to grow more slowly than the wild type and exhibit abnormally branched morphology, as previously shown with *Saccharomyces cerevisiae*, *Ustilago maydis*, and *Magnaporthe grisea* mutants (1, 29, 33).

Second, the BcPIE3 protein does not mediate drug- and fungicide-related toxicity effects in *B. cinerea*. The growth of the Δ36 strain was inhibited to a degree similar to that of the inhibition of the wild-type strain T4 in the presence of fungicides and drugs (Table 2).

Third, there is a similar example of a protein which, despite sharing basic structural features with EBPs, has no detectable Δ^8-Δ^7 isomerase or sigma ligand binding activity: the human EBP-like protein (47). The absence of both activities in the EBP-like protein is in agreement with the hypothesis of Jbilo and colleagues (31), who suggested that the sterol binding pocket present in the SI constitutes the sigma ligand binding site, regardless of the protein in which this pocket is found. The sterol and pharmacological profile of the Δ36 strain suggests the absence of both activities in BcPIE3 protein, although biochemical studies with the purified protein are required in order to confirm this hypothesis.

It is tempting to suggest that Δ^8-Δ^7 sterol isomerization is catalyzed by the *B. cinerea* ortholog of the yeast ERG2 protein, similar to that in *Magnaporthe grisea* and *Ustilago maydis* (29, 33). A putative ortholog of the *ERG2* gene was found in the *B. cinerea* genome (corresponding to Broad Institute protein identification no. BC1G_03303.1). The redundancy of EBD-encoding genes in *B. cinerea*, as well as the presence of a putative ERG2-like SI, suggests that the effects of the Bc*PIE3* disruption may have been masked by the activity of the remaining functional *B. cinerea* EBDPs (Fig. 6). It cannot be excluded that BcPIE3 plays a secondary role in the ergosterol biosynthesis pathway or has SI activity exclusively in the context of infection. A first step toward answering these questions may be a complementation experiment with an *ERG2*$^-$ yeast strain carrying the *ERG2* ortholog gene and each one of the three *B. cinerea EBDP* genes of the EBP phylogenetic cluster. It may also be interesting to verify whether BcPIE3, shown to

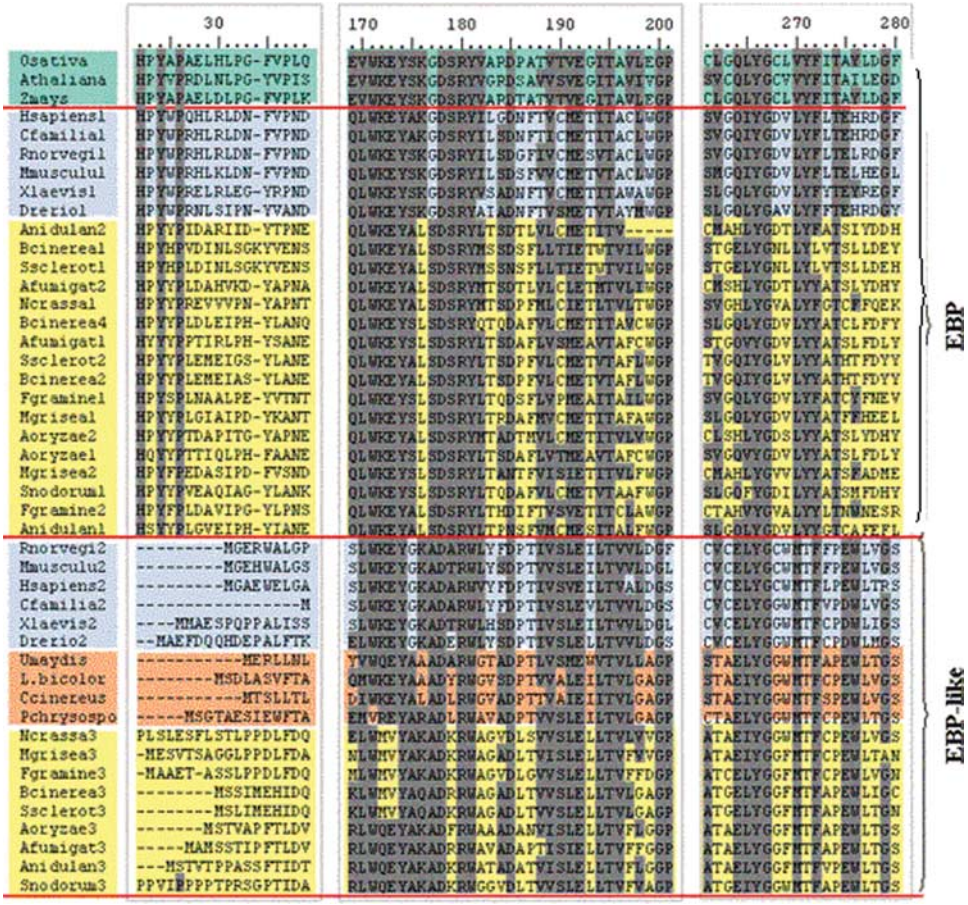

FIG. 7. Amino acid sequence alignment of eukaryotic EBDPs. Amino acid positions 22 to 39, 169 to 201, and 261 to 280 (according to BcPIE3 numbering) are shown. The threshold for residue shading was 55% identity or similarity using the substitution matrix Blosum 62. Coloring and entries correspond to those noted in the legend to Fig. 6. Horizontal red lines delimit plant, fungal, and mammalian groups. Conserved residues are shaded in grey.

be dispensable for ergosterol biosynthesis, nevertheless conserves the endoplasmic reticulum localization pattern of the human EBP (14), this topology being typical of enzymes of the sterol biosynthetic pathway.

The ancestral gene for EBDPs was duplicated in the common ancestor of fungi and animals. The phylogenetic analysis of proteins possessing the EBD showed that vertebrate and fungal EBDPs clustered together into two monophyletic groups (Fig. 6). The monophyly of the EBP-like clade, previously identified by Moebius and colleagues (47), is strongly supported, and fungal EBDPs encoded by single-copy genes were related to this clade (Fig. 6). All the other fungal EBDPs were more closely related to the vertebrate EBP group. The monophyly of the EBP clade was also well supported (Fig. 6). All the genomes of euascomycete species studied here contained at least two EBD-encoding genes, one encoding an EBP-like protein and one or more encoding an EBP. Plant genomes code for a single EBP, and basidiomycete genomes code for a single EBP-like protein, whereas yeasts and invertebrates do not contain any EBD-encoding gene at all. The most parsimonious hypothesis to explain this topology is that a duplication of the EBD-encoding gene took place in the ancestral lineage common to animals and fungi, after the split from plants. In this scenario, the EBD-encoding gene would then have been lost twice in the lineages of yeasts and invertebrates and once in the lineage of basidiomycetes. This hypothesis may be further tested once the genomes of zygomycetes, chytrids, and other species belonging to "intermediate" lineages (between those of ascomycetes and animals) are available.

Expansion of the EBP group: specific to euascomycete species. Of nine euascomycete species studied here, seven contained at least two distinct EBPs, that is, EBDPs that clustered into the EBP clade (Fig. 6). Moreover, for all euascomycete species, one EBDP systematically fell into the EBP-like clade. Overall, these findings are evidence that an expansion within the euascomycete EBP group took place via a new duplication (or a triplication in the case of *B. cinerea*). Given that no *EBDP* genes were detected in the genomes of hemiascomycetes and archaeascomycetes, whereas one EBP-like protein was found in each of the four basidiomycete species, the most parsimonious hypothesis is that the new duplication took place in the common ancestor of euascomycete species. Again, genomic data from lineages situated at the basis of the fungal evolutionary tree are needed to precisely date this probable duplication.

The superfamily of EBDPs: features and definition. The phylogenetic analysis of eukaryotic proteins that possess the EBD showed that these proteins are closely related, despite their apparent biochemical differences. The term EBDPs could be retained in the future, and EBDPs could be classified into the same protein superfamily (minimum identity observed in pairwise alignments, 19%; maximum identity observed, 89%). In view of the new protein alignments and the results of HCA of structures, we propose criteria for the definition of the EBDP superfamily.

The first criterion concerns the hydrophobic structure of the EBD and, more precisely, the systematic presence of five hydrophobic clusters, a common feature of all EBDPs studied here by HCA (data not shown). It is noteworthy that all EBDPs studied so far have been predicted to have only four TM domains based on current prediction algorithms (TMPred and Kyte-Doolittle). However, Hanner and colleagues (25) observed that the connecting loop between TM domains 3 and 4 in mammalian EBPs is highly hydrophobic. Here, HCA, which further permits the visualization of putative secondary structures (7), clearly highlighted the presence of this fifth domain (Fig. 5). Whether the HCA-predicted fifth hydrophobic cluster is a TM domain needs to be experimentally verified.

The second criterion is the presence of a highly conserved motif, highlighted by protein alignments (Fig. 7). Moebius and colleagues (46) had previously defined a conserved motif at the central loop between TM domains 2 and 3 of mammalian and plant EBPs, WKEYA/SKGDSRY; they further proposed that this motif is implicated in a proton/water delivery function or in the binding of an −OH group. Based on the protein alignment including fungal EBDPs, the consensus sequence for the central loop region becomes W/VXE/VYA/G/SXG/S/ADXRY/W. It is noteworthy that this motif is more conserved among the EBPs than among the EBP-like proteins (Fig. 7), despite the fact that the EBP clade comprises more proteins due to the expansion of the EBP clade in euascomycetes.

This new consensus motif, derived from the alignment of 42 EBDPs, could be used as a signature for the definition of the superfamily and the assignment of newly identified proteins as members. The most-conserved residues within the central loop region motif (Y, D, and R) (Fig. 5), as well as two more residues downstream, located in the fourth TM domain of all EBDPs, E^{197} and T^{200} (positions in the alignment) (Fig. 7), were defined previously to be critical for sterol isomerization (46). However, given that probably not all EBDPs are SIs, the consensus motif may not represent a unique biochemical function. The variability of residues within this motif may reflect the evolution of EBDPs toward novel functions. It may be a sign of adaptation to different ligands or different cellular environments.

Evolution of fungal EBPs and their functions: conclusions and questions. Gene duplication with subsequent divergence is the principal mechanism of the emergence of new functions during evolution (41, 34). On the other hand, inferring protein functions based on phylogenomic analysis can be complicated in the case of protein superfamilies (6). It will be interesting to further investigate the functional evolution of fungal *EBP* genes in the future. Our study provides evidence that the fungal EBP clade was subjected to lineage-specific expansion. The EBP phylogenetic cluster contains an additional member(s) in euascomycetes, but in vertebrates, the presence of single copies of *EBP* genes in the genomes has been conserved. BcPIE3, the first protein of this clade to be characterized, was shown to be dispensable for ergosterol biosynthesis in *B. cinerea*. If the SI activity in fungi is indeed encoded by *ERG2* orthologs, as shown for the euascomycete *Magnaporthe grisea* and the basidiomycete *Ustilago maydis* (29, 33), then fungal *EBP* genes may have acquired different functions.

A previous systematic analysis of lineage-specific expansions in five eukaryotic genomes showed that those related to organism-specific aspects such as pathogenicity are the most abundant (39). In the same line, BcPIE3, a member of the expanded fungal EBP clade, is a virulence factor for *B. cinerea*. We suggest that the BcPIE3 protein has a function related to the interactions with host plants. Functional characterization of EBPs from other pathogenic and nonpathogenic fungi in the future will contribute to an understanding of the grounds of the EBP clade expansion and, more generally, the evolution of the intriguing EBDP superfamily.

ACKNOWLEDGMENTS

We thank Tatiana Giraud for pertinent remarks on the phylogenetic analysis and Mathias Choquer for fruitful discussions.

This work was supported by grants from the National French Institute for Agronomic Research (INRA).

REFERENCES

1. **Ashman, W. H., R. J. Barbuch, C. E. Ulbright, H. W. Jarrett, and M. Bard.** 1991. Cloning and disruption of the yeast C-8 sterol isomerase gene. Lipids **26:**628–632.
2. **Bae, S., J. Seong, and Y. Paik.** 2001. Cholesterol biosynthesis from lanosterol: molecular cloning, chromosomal localization, functional expression and liver-specific gene regulation of rat sterol delta8-isomerase, a cholesterogenic enzyme with multiple functions. Biochem. J. **353:**689–699.
3. **Benghezal, M., G. Wasteneys, and D. A. Jones.** 2000. The C-terminal dilysine motif confers endoplasmic reticulum localization to type I membrane proteins in plants. Plant Cell **12:**1179–1201.
4. **Birney, E., M. Clamp, and R. Durbin.** 2004. GeneWise and Genomewise. Genome Res. **14:**988–995.
5. **Braverman, N., P. Lin, F. F. Moebius, C. Obie, A. Moser, H. Glossmann, W. R. Wilcox, D. L. Rimoin, M. Smith, L. Kratz, R. I. Kelley, and D. Valle.** 1999. Mutations in the gene encoding 3 beta-hydroxysteroid-Δ^8,Δ^7-isomerase cause X-linked dominant Conradi-Hünermann syndrome. Nat. Genet. **22:**291–294.
6. **Brown, D., and K. Sjölander.** 2006. Functional classification using phylogenomic inference. PLos Comput. Biol. **2:**e77.
7. **Callebaut, J., G. Labesse, P. Durand, A. Poupon, L. Canard, J. Chomilier, et al.** 1997. Deciphering protein sequence information through hydrophobic cluster analysis (HCA): current status and perspectives. Cell. Mol. Life Sci. **53:**621–645.
8. **Debieu, D., C. Gall, M. Gredt, J. Bach, C. Malosse, and P. Leroux.** 1992. Ergosterol biosynthesis and its inhibition by fenpropimorph in *Fusarium* species. Phytochemistry **31:**1223–1233.
9. **Debieu, D., J. Bach, A. Lasseron, C. Malosse, and P. Leroux.** 1998. Effects of sterol biosynthesis inhibitor fungicides in the phytopathogenic fungus, *Nectria haematococca*: ergosterol depletion versus precursor or abnormal sterol accumulation as the mechanism of fungitoxicity. Pestic. Sci. **54:**157–167.
10. **Debieu, D., J. Bach, A. Arnold, S. Brousset, M. Gredt, M. Taton, A. Rahier, C. Malosse, and P. Leroux.** 2000. Inhibition of ergosterol biosynthesis by morpholine, piperidine, spiroketalamine fungicides in *Microdochium nivale*: effect on sterol composition and sterol Δ^8-Δ^7 isomerase activity. Pestic. Biochem. Physiol. **67:**85–94.
11. **Debieu, D., J. Bach, M. Hugon, C. Malosse, and P. Leroux.** 2001. The hydroxyanilide fenhexamid, a new sterol biosynthesis inhibitor efficient against the plant pathogenic fungus *Botryotinia fuckeliana* (*Botrytis cinerea*). Pest Manag. Sci. **57:**1060–1067.
12. **Dellaporta, S. L., J. Wood, and J. B. Hicks.** 1983. A plant DNA minipreparation: version 2. Plant Mol. Biol. Rep. **1:**19–21.
13. **Derry, J. M., E. Gormally, G. D. Means, W. Zhao, A. Meindl, R. I. Kelley, Y. Boyd, and G. E. Herman.** 1999. Mutations in a Δ^8-Δ^7 sterol isomerase in the tattered mouse and X-linked dominant chondrodysplasia punctata. Nat. Genet. **22:**286–290.
14. **Dussossoy, D., P. Carayon, S. Belugou, D. Feraut, A. Bord, C. Goubet, C.**

Roque, H. Vidal, T. Combes, G. Loison, and P. Gasellas. 1999. Colocalization of sterol isomerase and sigma$_1$ receptor at endoplasmic reticulum and nuclear envelope level. Eur. J. Biochem. **263:**377–385.
15. **Elad, Y., B. Williamson, P. Tudzynski, and N. Delen.** 2004. *Botrytis* spp. and diseases they cause in agricultural systems: an introduction, p. 1–8. *In* Y. Elad, B. Williamson, P. Tudizynski, and N. Delen (ed.), *Botrytis*: biology, pathology and control. Kluwer Academic Publishers, Dordrecht, The Netherlands.
16. **Felsenstein, J.** 1989. PHYLIP: Phylogeny Inference Package (version 3.2). Cladistics **5:**164–166.
17. **Gaboriaud, C., V. Bissery, T. Benchetrit, and J.-P. Mornon.** 1987. Hydrophobic cluster analysis. An efficient new way to compare and analyze amino-acid sequences. FEBS Lett. **224:**149–155.
18. **Gioti, A., A. Simon, P. Le Pêcheur, C. Giraud, J. M. Pradier, M. Viaud, and C. Levis.** 2006. Expression profiling of *Botrytis cinerea* genes identifies three patterns of up-regulation *in planta* and an FKBP12 protein affecting pathogenicity. J. Mol. Biol. **358:**372–386.
19. **Gourgues, M., P.-H. Clergeot, C. Veneault, J. Cots, S. Sibuet, A. Brunet-Simon, C. Levis, T. Langin, and M. H. Lebrun.** 2002. A new class of tetraspanins in fungi. Biochem. Biophys. Res. Commun. **297:**1197–1204.
20. **Gourgues, M., A. Brunet-Simon, M.-H. Lebrun, and C. Levis.** 2004. The tetraspanin BcPLS1 is required for appressorium-mediated penetration of *Botrytis cinerea* into host plant leaves. Mol. Microbiol. **51:**619–629.
21. **Grange, D. K., L. E. Kratz, N. E. Braverman, and R. I. Kelley.** 2000. CHILD syndrome caused by deficiency of 3β-hydroxysteroid-Δ^8,Δ^7-isomerase. Am. J. Med. Genet. **90:**328–335.
22. **Grebenok, R. J., T. E. Ohnmeiss, A. Yamamoto, E. D. Huntley, D. W. Galbraith, and D. D. Penna.** 1998. Isolation and characterization of an *Arabidopsis thaliana* C-8,7 sterol isomerase: functional and structural similarities to mammalian C-8,7 sterol isomerase/emopamil-binding protein. Plant Mol. Biol. **38:**807–815.
23. **Guindon, S., F. Lethier, P. Duroux, and O. Gascuel.** 2005. PHYML Online—a web server for fast maximum likelihood-based phylogenetic inference. Nucleic Acids Res. **33**(Web server issue)**:**W557–W559.
24. **Hall, T. A.** 1999. BioEdit: a user-friendly biological sequence alignment editor and analysis program for Windows 95/98/NT. Nucleic Acids Symp. Ser. **41:**95–98.
25. **Hanner, M., F. F. Moebius, F. Weber, M. Grabner, J. Striessnig, and H. Glossmann.** 1995. Phenylalkylamine Ca^{2+} antagonist binding protein: molecular cloning, tissue distribution and heterologous expression. J. Biol. Chem. **270:**7551–7557.
26. **Has, C., L. Bruckner-Tuderman, D. Müller, M. Floeth, E. Folkers, D. Donnai, and H. Traupe.** 2000. The Conradi-Hünermann-Happle syndrome (CDPX2) and emopamil binding protein: novel mutations, and somatic and gonadal mosaicism. Hum. Mol. Genet. **9:**1951–1955.
27. **Hofmann, K., and W. Stoffel.** 1993. TMbase: a database of membrane spanning protein segments. Biol. Chem. Hoppe-Seyler **374:**166.
28. **Jackson, M. R., T. Nilsson, and P. A. Peterson.** 1990. Identification of a consensus motif for retention of transmembrane proteins in the endoplasmic reticulum. EMBO J. **9:**3153–3162.
29. **James, C. S., R. S. Burden, R. S. T. Loeffler, and J. A. Hargreaves.** 1992. Isolation and characterization of polyene-resistant mutants from the maize smut pathogen, Ustilago maydis, defective in ergosterol biosynthesis. J. Gen. Microbiol. **138:**1437–11443.
30. **Jarwis, W. R.** 1977. Canada Department of Agriculture monograph 15. *Botryotinia* and *Botrytis* species—taxonomy, physiology and pathogenicity: a guide to literature, p. 195. Canada Department of Agriculture, Harrow, Ontario, Canada.
31. **Jbilo, O., H. Vidal, R. Paul, N. De Nys, M. Bensaid, S. Silve, P. Carayon, D. Davi, S. Galiègue, B. Bourrié, J.-C. Guillemot, P. Ferrara, G. Loison, J.-P. Maffrand, G. Le Fur, and P. Casella.** 1997. Purification and characterization of the human SR 31747A-binding protein. A nuclear membrane protein related to yeast sterol isomerase. J. Biol. Chem. **272:**27107–27115.
32. **Jones, D. T., W. R. Taylor, and J. M. Thornton.** 1992. The rapid generation of mutation data matrices from protein sequences. Comput. Appl. Biol. Sci. **8:**275–282.
33. **Keon, J. P. R., C. S. James, S. Court, C. Baden-Daintree, A. M. Bailey, R. S. Burden, M. Bard, and J. A. Hargreaves.** 1994. Isolation of the ERG2 gene, encoding sterol $\Delta 8 \rightarrow \Delta 7$ isomerase, from the rice blast fungus *Magnaporthe grisea* and its expression in the maize smut pathogen *Ustilago maydis*. Curr. Genet. **25:**531–537.
34. **Kondrashov, F. A., I. B. Rogozin, Y. I. Wolf, and E. V. Koonin.** 2002. Selection in the evolution of gene duplication. Genome Biol. **3:**R8.
35. **Kyte, J., and R. Doolittle.** 1982. A simple method for displaying the hydropathic character of a protein. J. Mol. Biol. **157:**105–132.
36. **Laggner, C., C. Schieferer, B. Fiechtner, G. Poles, R. Hoffmann, H. Glossmann, T. Langer, and F. F. Moebius.** 2005. Discovery of high-affinity ligands of σ_1 receptor, ERG2 and emopamil binding protein by pharmacophore modeling and virtual screening. J. Med. Chem. **48:**4754–4764.
37. **Lei, Z., and Y. Dai.** 2005. An SVM-based system for predicting protein subnuclear localizations. BMC Bioinformatics **6:**291. doi:10.1186/1471-2105-6-291.
38. **Leroux, P., F. Chapeland, D. Desbrosses, and M. Gredt.** 1999. Patterns of cross-resistance to fungicides in *Botryotinia fuckeliana* (*Botrytis cinerea*) isolates from French vineyards. Crop Prot. **18:**687–697.
39. **Lespinet, O., Y. I. Wolf, E. V. Koonin, and L. Aravind.** 2006. The role of lineage-specific gene family expansion in the evolution of eukaryotes. Genome Res. **12:**1048–1059.
40. **Levis, C., M. Dutertre, D. Fortini, and Y. Brygoo.** 1997. Transformation of *Botrytis cinerea* with the structural nitrate reductase gene (niaD) shows a high frequency of homologous recombination. Curr. Genet. **32:**157–162.
41. **Lynch, M., and J. S. Conery.** 2000. The evolutionary fate and consequences of duplicated genes. Science **290:**1151–1155.
42. **Marchler-Bauer, A., and S. H. Bryant.** 2004. CD-Search: protein domain annotations on the fly. Nucleic Acids Res. **32:**W327–331.
43. **Moebius, F. F., G. G. Burrows, J. Striessnig, and H. Glossmann.** 1993. Biochemical characterization of a 22-kDa high affinity antiischemic drug-binding polypeptide in the endoplasmic reticulum of guinea pig liver: potential common target for antiischemic drug action. Mol. Pharmacol. **43:**139–148.
44. **Moebius, F. F., K. Bermoser, R. J. Reiter, M. Hanner, and H. Glossman.** 1996. Yeast sterol C8–C7 isomerase: identification of a high affinity binding site for enzyme inhibitors. Biochemistry **35:**16871–16878.
45. **Moebius, F. F., R. J. Reiter, K. Bermoser, H. Glossmann, S. Y. Cho, and Y.-K. Paik.** 1998. Pharmacological analysis of sterol Δ8-Δ7 isomerase proteins with [^{3}H]ifenprodil. Mol. Pharmacol. **54:**591–598.
46. **Moebius, F. F., K. E. M. Soellner, B. Fiechtner, C. W. Huck, G. Bonn, and H. Glossmann.** 1999. Histidine^{77}, glutamic acid^{81}, glutamic acid^{123}, threonine^{126}, asparagine^{194} and tryptophan^{197} of the human emopamil binding protein are required for in vivo sterol Δ^8-Δ^7 isomerization. Biochemistry **38:**1119–1127.
47. **Moebius, F. F., B. U. Fitzky, G. Wietzorrek, A. Haidekker, A. Eder, and H. Glossmann.** 2003. Cloning of an emopamil-binding protein (EBP)-like protein that lacks sterol Δ^8-Δ^7 isomerase activity. Biochem. J. **374:**229–237.
48. **Pawagi, A. B., J. Wang, M. Silverman, R. A. Reithmeier, and C. M. Deber.** 1994. Transmembrane aromatic amino acid distribution in P-glycoprotein: a functional role in broad substrate specificity. J. Mol. Biol. **235:**554–564.
49. **Rahier, A., and M. Taton.** 1996. Sterol biosynthesis: strong inhibition of maize $\Delta^{5,7}$-sterol Δ^7 reductase by novel 6-aza-*B*-homosteroids and other analogues of a presumptive carbocationic intermediate of the reduction reaction. Biochemistry **35:**7069–7076.
50. **Sambrook, J., E. F. Fritsch, and T. Maniatis.** 1989. Molecular cloning: a laboratory manual, vol. 3. Cold Spring Harbor Laboratory Press, Cold Spring Harbor, NY.
51. **Schneegurt, M. A., and M. Henry.** 1992. Effects of piperalin and fenpropimorph on sterol biosynthesis in *Ustilago maydis*. Pestic. Biochem. Physiol. **43:**45–52.
52. **Silve, S., P. H. Dupuy, C. Labit-Lebouteiller, M. Kaghad, P. Chalon, A. Rahier, M. Taton, J. Lupker, D. Shire, and G. Loison.** 1996. Emopamil-binding protein, a mammalian protein that binds a series of structurally diverse neuroprotective agents, exhibits Δ^8-Δ^7 sterol isomerase activity in yeast. J. Biol. Chem. **271:**22434–22440.
53. **Sweigard, J., F. Chumley, A. Carroll, L. Farrall, and B. Valent.** 1997. A series of vectors for fungal transformation. Fungal Genet. Newsl. **44:**52–53.
54. **Swofford, D. L.** 1998. PAUP*: Phylogenetic Analysis Using Maximum Parsimony (*and Other Methods), version 4.0. Sinauer Associates Inc., Sunderland, MA.
55. **Tatusov, R. L., E. V. Koonin, and D. J. Lipman.** 1997. A genomic perspective on protein families. Science **278:**631–637.
56. **Thordal-Christensen, H., Z. Shang, Y. Wei, and D. B. Collinge.** 1997. Subcellular localization of H_2O_2 in plants. H_2O_2 accumulation in papillae and hypersensitive response during the barley powdery mildew interaction. Plant J. **11:**1187–1194.
57. **Viaud, M., A. Brunet-Simon, Y. Brygoo, J.-M. Pradier, and C. Levis.** 2003. Cyclophilin A and calcineurin functions investigated by gene inactivation, cyclosporin A inhibition and cDNA arrays approaches in the phytopathogenic fungus *Botrytis cinerea*. Mol. Microbiol. **50:**1451–1465.
58. **Volkman, J. K.** 2003. Sterols in microorganisms. Appl. Microbiol. Biotechnol. **60:**495–506.
59. **Woodcock, S., J.-P. Mornon, and B. Henrissat.** 1992. Detection of secondary structure elements in proteins by hydrophobic cluster analysis. Protein Eng. **5:**629–635.